



Contents lists available at ScienceDirect

Medical Image Analysis

journal homepage: www.elsevier.com/locate/media

A classifying registration technique for the estimation of enhancement curves of DCE-CT scan sequences

Mohamed Hachama^a, Agnès Desolneux^b, Charles A. Cuenod^c, Frédéric J.P. Richard^{b,*}

^a Centre Universitaire Khemis Miliana, Route Teniat el Had, Ain Defla, Algeria

^b University Paris Descartes, MAP5, CNRS UMR 8145, 45, rue des Sains-Peres, 75270 Paris Cedex, France

^c University Paris Descartes, LRI-EA4062, APHP – European Hospital Georges Pompidou, Service of Radiology, 10 rue Leblanc, 75015 Paris, France

ARTICLE INFO

Article history:

Received 30 July 2008

Received in revised form 24 September 2009

Accepted 8 December 2009

Available online xxxxx

Keywords:

Image registration

Dynamic Contrast-Enhanced images

Enhancement curves estimation

ABSTRACT

In this paper, we propose a new technique for the estimation of contrast enhancement curves of Dynamic Contrast-Enhanced sequences, which takes the most from the interdependence between this estimation problem and the registration problem raised by possible movements occurring in sequences. The technique solves the estimation and registration problems simultaneously in an iterative way. However, unlike previous techniques, a pixel classification scheme is included within the estimation so as to compute enhancement curves on pixel classes instead of single pixels. The classification scheme is designed using a descendant hierarchical approach. Due to this tree approach, the number of classes is set automatically and the whole technique is entirely unsupervised. Moreover, some specific prior information about the shape of enhancement curves are included in the splitting and pruning steps of the classification scheme. Such an information ensures that created classes include pixels having homogeneous and relevant enhancement properties. The technique is applied to DET-CT scan sequences and evaluated using ground truth data. Results show that classifications are anatomically sound and that contrast enhancements are accurately estimated from sequences.

© 2009 Elsevier B.V. All rights reserved.

1. Introduction

The past few years have witnessed an increase in the use of dynamic imaging modalities such as Dynamic Contrast-Enhanced Computed Tomography (DCE-CT) (Miles, 2003) and Magnetic Resonance Imaging (DCE-MRI) (O'Connor et al., 2007). Such modalities generate time series of 2D or 3D images of human organs, which are relevant for the diagnosis and the management of cancers (Cuénod et al., 2006; Kuhl, 2007; Padhani, 2002; Zahra et al., 2007), ischemic diseases such as stroke (Wintermark, 2005), myocardial ischemia (Judd et al., 1995), and inflammation. In such sequences, a contrast agent is used to distinguish and enhance different organ tissues which are characterized by their absorption of contrast agent through time (Kaiser, 1990; Stack et al., 1990).

However, the clinical analysis of these images usually requires computer processing tools facilitating the image interpretation. As related to contrast agent concentration in tissue, a temporal intensity evolution of a single or a group of pixels, called enhancement curve, is usually used for the automation of lesion detection and diagnosis (Hayton et al., 1997; Mussurakis et al., 1995). Such curves are also used to define parametric maps of some extracted

parameters to get a functional segmentation of images. However, the analysis of enhancement curves faces two main problems: the presence of noise and movements of patients.

Sequences of DCE-CT-scans have poor signal-to-noise ratio due to the limited irradiation dose used for sequential acquisition and are subject to tomographic reconstruction errors. Hence, there is a need to denoise enhancement curves obtained directly from images. For that, some authors proposed to estimate the contrast enhancement curves using some mathematical prior models which define possible forms of curves (Tofts, 1997; Hayton et al., 1997; Buonaccorsi et al., 2006; Moate et al., 2004; Henkjan et al., 2001). There are two main classes of prior models: biophysical-based models and mathematical models. The first class contains models derived from a pharmacokinetic modeling of the contrast agent concentration and circulation in two interacting compartments: namely, blood plasma and extra-vascular–extracellular space EES (Tofts, 1997; Hayton et al., 1997; Buonaccorsi et al., 2006). The resulting models depend on some parameters which are assumed to be related to the physical process and can be estimated using statistical techniques (Schmid et al., 2005; Hayton et al., 1997; Buonaccorsi et al., 2006). The second class of models is based on the use of heuristic parametric curves which reproduce main features of an expected curve such as the base-line signal, the enhancement rate, the time-to-peak, the peak of enhancement,

* Corresponding author.

E-mail address: frederic.richard@parisdescartes.fr (F.J.P. Richard).

or the final slope (Moate et al., 2004; Henkjan et al., 2001; Mussurakis et al., 1995). Although this second class is not necessarily predictive, it is more generic and it does not require any assumption or inference about the underlying physiology.

Since the acquisition of a DCE sequence takes some minutes, patient movements and physiologic motion (caused, for instance, by breathing, heartbeat, muscle contractions) cannot be avoided and generate differences from non-pathological origins between images which must be corrected before any curve analysis. Image registration, which maps images to a common space, is usually applied to correct geometric differences between images. But, in most classical registration techniques, the same relation between pixel intensities is assumed for the whole image (Roche et al., 2000). Such an assumption implies that two pixels with similar intensities in an image have similar intensities in another image. This hypothesis is not valid in many cases. In DCE images, normal tissues and lesions have different enhancements after injection even though their intensities are similar before injection. One can also observe dynamic enhancement differences between benign and malignant tumors. In other words, the contrast enhancement varies locally depending on the tissue type and not exclusively on initial intensities.

In Rougon et al. (2005), Rougon et al. adapted the f-information criterion for the registration of a first pre-contrast injection image to a second post-contrast image. Assuming that the first image can be segmented into some regions having homogeneous enhancement properties, they defined a regionalized criterion based on f-information on each region. Such an approach requires a preliminary segmentation of images into anatomical components of interest. But, in our DET-CT problem, it is difficult to obtain such a segmentation before image registration. The sequence segmentation needs to be done according to dynamic enhancement properties of pixels, which are better estimated using the registered images. In other words, not only the sequence registration requires taking into account a local information about pixel enhancements but also the estimation of enhancements requires the sequence to be registered. Therefore, the enhancement estimation and the registration are two interdependent problems.

For that reason, some authors proposed to solve the two problems simultaneously. In Hayton et al. (1997), the authors used a pharmacokinetic model to describe enhancement for each pixel x by a temporal curve $C_x(t)$. They used an optical flow-based technique for the registration of each image of an original sequence observed at time t to an ideal image I^t where $I^t(x) = C_x(t)$ for all pixels x . In their technique, registration and estimation are iterated successively: registered images are used for the enhancement curve estimation and the estimated curves are used to generate ideal images $I^t(x)$ to which original images are registered. This technique was applied for the improvement of lesion detection in mammography. A similar idea was used in Buonaccorsi et al. (2006) for the registration of axial volumes within the abdomen to synthetic volumes built upon estimated enhancement curves. As in Hayton et al. (1997), enhancement curves are estimated locally for each pixel. Such an estimation is both time-consuming and noise sensitive. In Xiaohua et al. (2005), Xiaohua et al. proposed a Bayesian framework which is based on a *Maximum A Posteriori* estimation and performs simultaneously registration of breast DCE-MRI images and segmentation of non-fat tissues into three regions: normal tissue, benign lesions and malignant lesions. In this work, the authors estimate dynamic enhancement curves and classify pixels depending on some features computed using enhancement curves (early-phase enhancement rate, and intermediate and final slope). Since curve estimation is done for each pixel, their technique presents the same drawbacks as those in Buonaccorsi et al. (2006) and Hayton et al. (1997). Moreover, the number of classes has to be set manually.

In this paper, we propose a new technique for the estimation of enhancement curves of DCE-CT scan sequences. This technique takes the most from the interdependence between this estimation problem and the registration problem posed by possible movements occurring in sequences. Similarly to Buonaccorsi et al. (2006), Hayton et al. (1997) and Xiaohua et al. (2005), it solves the estimation and registration problems simultaneously in an iterative way. However, the main departure of our techniques from previous ones is the use of a pixel classification scheme within the estimation procedure. Due to the introduction of this scheme, enhancement curves can be estimated on pixel classes instead of single pixels. This new feature makes the enhancement estimation more robust to noise than in pixel-based techniques and reduces the computation time. Let us also mention the work of Lorenzo et al. (2006) where enhancement curves are also used as spatio-temporal attributes for the registration and the segmentation of cardiac perfusion MRI. The technique, which is semi-automatic, is based on the evolution of level sets according to some distances between enhancement curves of each pixel and those of user-determined seed points.

Moreover, in our approach, the number of classes is set automatically. Consequently, the whole technique is entirely unsupervised. The classification scheme is designed using a descendant hierarchical approach. It includes some specific knowledge about the shape of enhancement curves. Enhancement curves estimated on classes are described using heuristic parametric curves similar to those used in Moate et al. (2004), Henkjan et al. (2001) and Mussurakis et al. (1995). This description of class curves is used in the splitting and pruning steps of the classification scheme. It enforces spatio-temporal constraints on classes so that they correspond to parts of the sequence having homogeneous and realistic enhancement properties.

In brief, the benefit of our technique is twofold: (i) improved estimation of local contrast enhancement curves, thanks to the use of a nonlocal estimation support (i.e. the class support sets) and of a parametric prior enhancement model; and (ii) improved registration thanks to the use of a noise-attenuated regionalized template model which implicitly introduces some geometric information in an iconic registration criterion.

2. Method

Let Ω be a continuous domain, Ω_d an associated discrete grid on which images are observed ($\text{Card}(\Omega_d) = N$), and J^t the image of the original sequence observed at time t . Our technique aims to estimate from the original sequence $(J^t)_{t \in T}$, an ideal image sequence $(I^t)_{t \in T}$ where the noise is attenuated and patient movements are compensated for. The ideal sequence will be called the "temporal template". For each $t \in T$, I^t is the template frame at time t defined as a real-value function on Ω .

2.1. Template definition

We assume that pixels of the domain can be partitioned into K homogeneous classes having specific dynamic enhancements: $\Omega_d = \cup_{k=1}^K \Omega^k$. Such an hypothesis is true in our medical application where pixels belonging to the same tissue type have similar enhancement properties. To introduce some priors on dynamic enhancement curves, we further assume that these curves belong to a class of heuristic models (Moate et al., 2004), which have the following shape:

$$C(t) = \frac{p_2 + p_5 t}{1 + e^{-(p_4(t-p_3))}} + p_1. \quad (1)$$

In such models, the parameters $(p_i)_{1 \leq i \leq 5}$ characterize the curve shape. The geometric interpretation of these parameters and their links with the clinically relevant parameters (baseline, time-to-

peak, enhancement rate, peak of enhancement, etc.) are given in Moate et al. (2004). In Fig. 1, we show an example of the fitting of the heuristic model (1) to an empirical curve computed from images.

Taking into account both pixel classes and their associated enhancement curves, denoted by $(C^k)_k$, the temporal template can be defined for all $t \in T$, $k \in \{1, \dots, K\}$ and $x \in \Omega^k$ as

$$I^t(x) = C^k(t) = \frac{p_2^k + p_3^k t}{1 + \exp(-p_4^k(t - p_3^k))} + p_1^k. \quad (2)$$

The temporal template is represented in Fig. 2. The template frame I^t at time t will be registered to the observed image J^t . The deformation making the two images similar will be denoted by ϕ^t ($I^t \circ \phi^t \sim J^t$).

2.2. Technique description

On the one hand, the estimation of the temporal template requires a movement correction by image registration. On the other hand, the image registration uses the temporal template so as to take into account contrast changes. As described in Fig. 3, our technique enables to perform the two tasks (estimation and registration) simultaneously by iterating two interacting blocks, called blocks (R) and (T).

The block (R) concerns image registration. The temporal template I estimated from the block (T) is registered to observed images $(J^t)_{t \in T}$, frame by frame (i.e. I^t is registered to J^t for all t). The output of the block (R) is a set of deformations $(\phi^t)_{t \in T}$ obtained from registrations and defined later. These deformations are the input of the block (T), which is devoted to the temporal template estimation. The block (T) combines a pixel classification and an estimation of enhancement curve of each class. The pixel features used in the classification are the pixel enhancement curves $(C_x)_{x \in \Omega_d}$ defined for all t in T as

$$C_x(t) = J^t((\phi^t)^{-1}(x)), \quad (3)$$

where $(\phi^t)^{-1}$ is the inverse map of ϕ^t . These local curves computed at each pixel are different from the class curves $(C^k)_{k=1}^K$ (also called class centers), which are of the parametric form (1). The two blocks are further presented in the next paragraphs.

2.3. Block (T)

In this section, we describe the combined classification and estimation technique used for the estimation of the temporal template. Assuming that some deformations ϕ^t are given for all t , pixels $x \in \Omega_d$ are classified according to their associated pixel enhancement curves $(C_x)_{x \in \Omega_d}$ (Eq. (3)). The classification technique

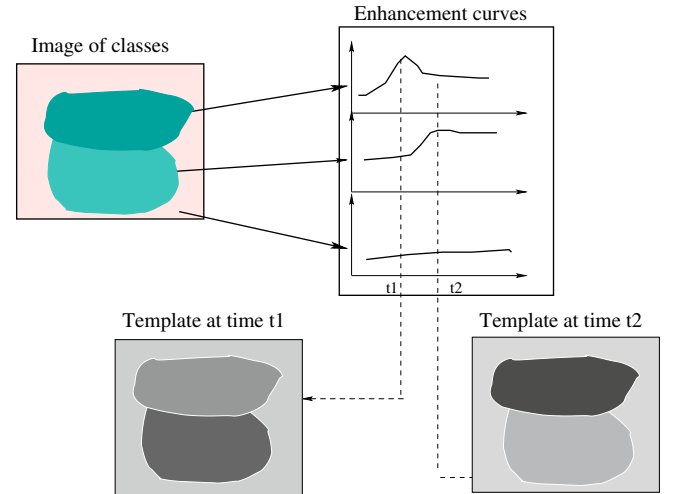


Fig. 2. The temporal template construction based on pixel classes and associated enhancement curves.

is composed of three successive steps (an initialization step, a tree classification and a pruning step) described next.

2.3.1. Initialization step

In our application (axial abdominal and thoracic CT-scans), we use the specificities of the images to set some initial classes. We apply a simple thresholding procedure to the first image of the sequence in order to fix three initial classes ('air', 'compact bone', and 'others'). In the first image, compact bones regions have the highest intensities whereas air regions have the lowest. Hence, both classes can be easily detected using both low and high thresholds. Threshold values are fixed for all CT-scan experiments according to the Hounsfield scale (−1000 for the air, and 4000 for the compact bones). In addition, since these classes do not absorb contrast agent, their intensities tend to remain constant with time. Hence, centers of these classes are set as constants.

For other applications, this initialization step should be modified taking into account the specificities of the images. If no prior information is available, it can even be skipped by choosing an ad hoc classification containing a single class.

2.3.2. Tree classification

In this step, we use a top-down hierarchical classification. As illustrated in Fig. 4, this technique generates a tree structure of embedded pixel classes by splitting classes successively at different levels of the tree. The initial classification obtained in the first

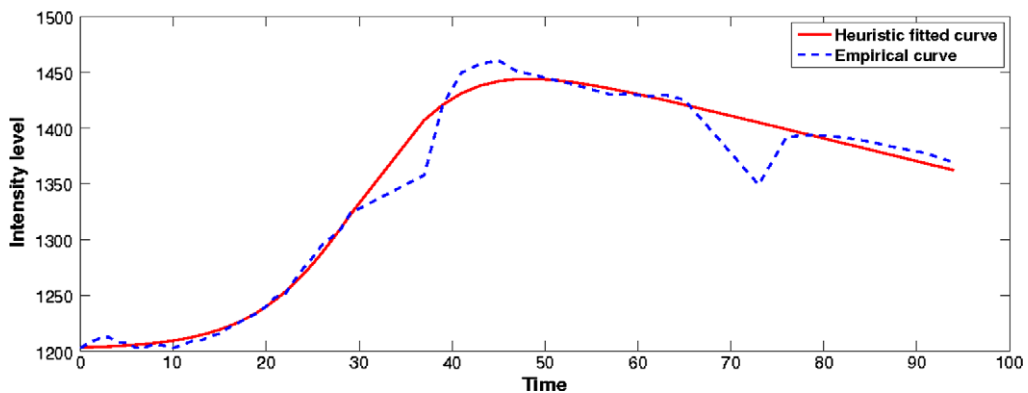


Fig. 1. Fitting the heuristic model (1) to an empirical curve.

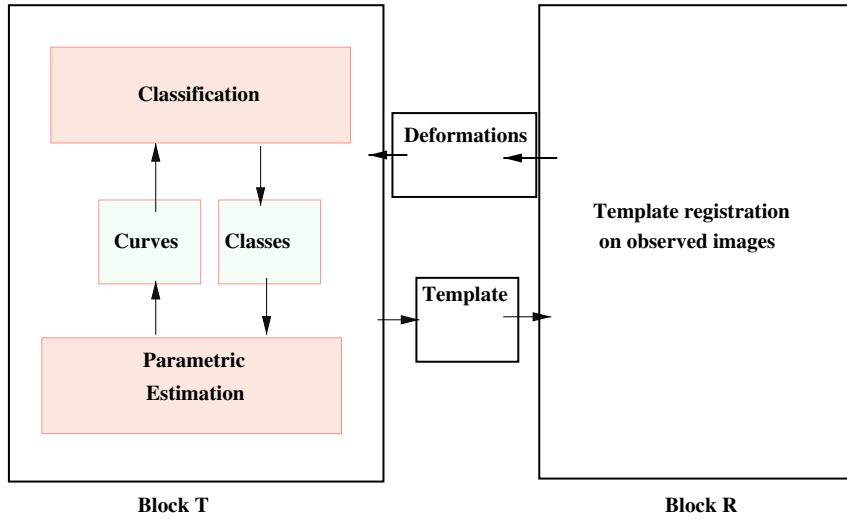


Fig. 3. The two interacting blocks of the technique: the image registration block (*R*) and the temporal template estimation (*T*). The latter interleaves pixel classification and estimation of the enhancement curve for each class.

step is associated to the superior level (level 1). Assuming that the technique has built the h highest levels, the level $h + 1$ of the tree is then constructed as follows. Each class of the level h is first divided into two candidate clusters using a parametric K-means, which will be described next. Then, if a candidate class is well separated from all other classes, it is accepted as a new class and the class of level h which it originates from is removed. Otherwise, the originate class is considered as non dividable. The criterion used for defining a distance between classes is the minimum between the class centers over the number of images $|T|$. A class is considered well separated from another class if the distance is above a threshold equal to $0.1\sigma|T|$, where σ is the noise standard deviation and T is the number of images in the sequence.

For building the classification tree, we modified the usual K-means technique (Duda et al., 2000) in order to take into account some prior knowledge about the class centers. The modified technique iterates two successive steps until convergence.

- (1) Compute each class center by fitting a parametric curve of the shape given by Eq. (1) to all enhancement curves of pixels of the class (or, equivalently, to their arithmetic average) according to a least square criterion.
- (2) Classify each pixel into the nearest class according to distances between class centers and the enhancement curve associated with the pixel.

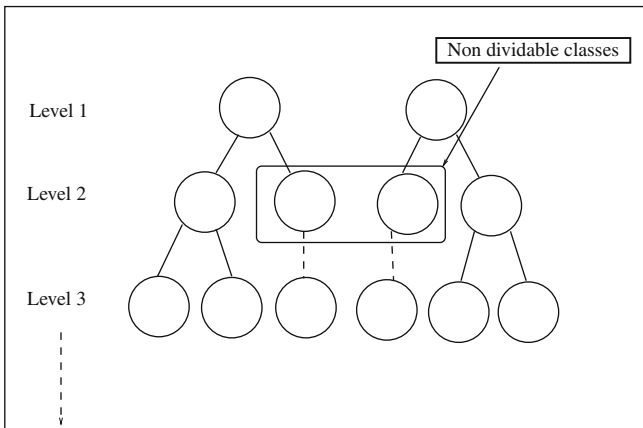


Fig. 4. Descendant hierarchical classification.

2.3.3. Pruning step

At the end of the construction of the tree, we have a pruning step to remove possible remaining inconsistent classes. A pixel class with center C is considered to be inconsistent when its mean contrast change is negative:

$$\sum_t (C(t) - C(t_0)) < 0,$$

where t_0 is the initial time of interval T . Here we used a simple criterion which can be replaced by other medically-based criteria. When a class is removed, its pixels are affected to the remaining class for which the distance between the center and the pixel enhancement curve is the lowest.

2.4. Image registration

So as to register a template frame I^t to a corresponding observed image J^t , we compute a deformation ϕ^t , defined as a mapping of Ω onto Ω minimizing an energy of the form

$$E(\phi^t) = R(\phi^t) + S(\phi^t), \quad (4)$$

where S is the similarity term defined as

$$S(\phi^t) = \int_{\Omega} (J^t(x) - I^t(\phi^t(x)))^2 dx \quad (5)$$

and R is an elastic potential

$$R(\phi^t) := \frac{1}{2} \sum_{i=1}^2 \sum_{j=1}^2 \int_{\Omega} \frac{\lambda}{2} \frac{\partial u_i^t(x)}{\partial x_i} \frac{\partial u_j^t(x)}{\partial x_j} + \frac{\mu}{4} \left(\frac{\partial u_i^t(x)}{\partial x_j} + \frac{\partial u_j^t(x)}{\partial x_i} \right)^2 dx. \quad (6)$$

Constants λ and μ , which are called the Lamé coefficients in elasticity, are set once for all in all experiments ($\lambda = 10^{-15}$ and $\mu = 20$) and $u^t = (u_1^t, u_2^t) = \phi^t - Id$ are displacements associated to deformations. The second term S of the energy expresses some similarity constraints between observed images and template frames, implying that observed images and estimated template have similar intensities at each time t . Such an assumption is guaranteed if the template includes a good estimation of contrast changes observed in images. The registration of all images is obtained by minimizing the following energy:

$$\mathbf{E}(\phi^1, \dots, \phi^T) = \sum_{t=1}^T E(\phi^t) = \sum_{t=1}^T R(\phi^t) + \sum_{t=1}^T S(\phi^t). \quad (7)$$

For solving numerically this problem, we use the FREEFEM++ software Hecht (2008) which enables to solve partial differential equations using the finite element method. For the discretization of this optimisation problem, we use the finite element technique (Polynomial Lagrange elements $P1$) to approximate the continuous deformations by a finite combination of local functions (Hachama et al., 2006). We then apply a gradient descent technique on the set of coefficients defining this combination. So as to speed up the technique convergence, we have used a multigrid approach, which consists of first initializing deformations with coarse

approximation using a small number of vertices and then increasing this number when necessary. In practice, for an image of size 256×256 , we have used five resolution levels with 15^2 , 30^2 , 45^2 , 60^2 , and 65^2 vertices, respectively. At each resolution, we make four iterations of the gradient descent to estimate the coordinate of displacements on each vertex. More details about the discretization and the Euler equations can be found in Hachama (2008).

3. Results

We applied our technique to 11 sequences of DCE-CT-scans from four different patients. We first describe in details results ob-

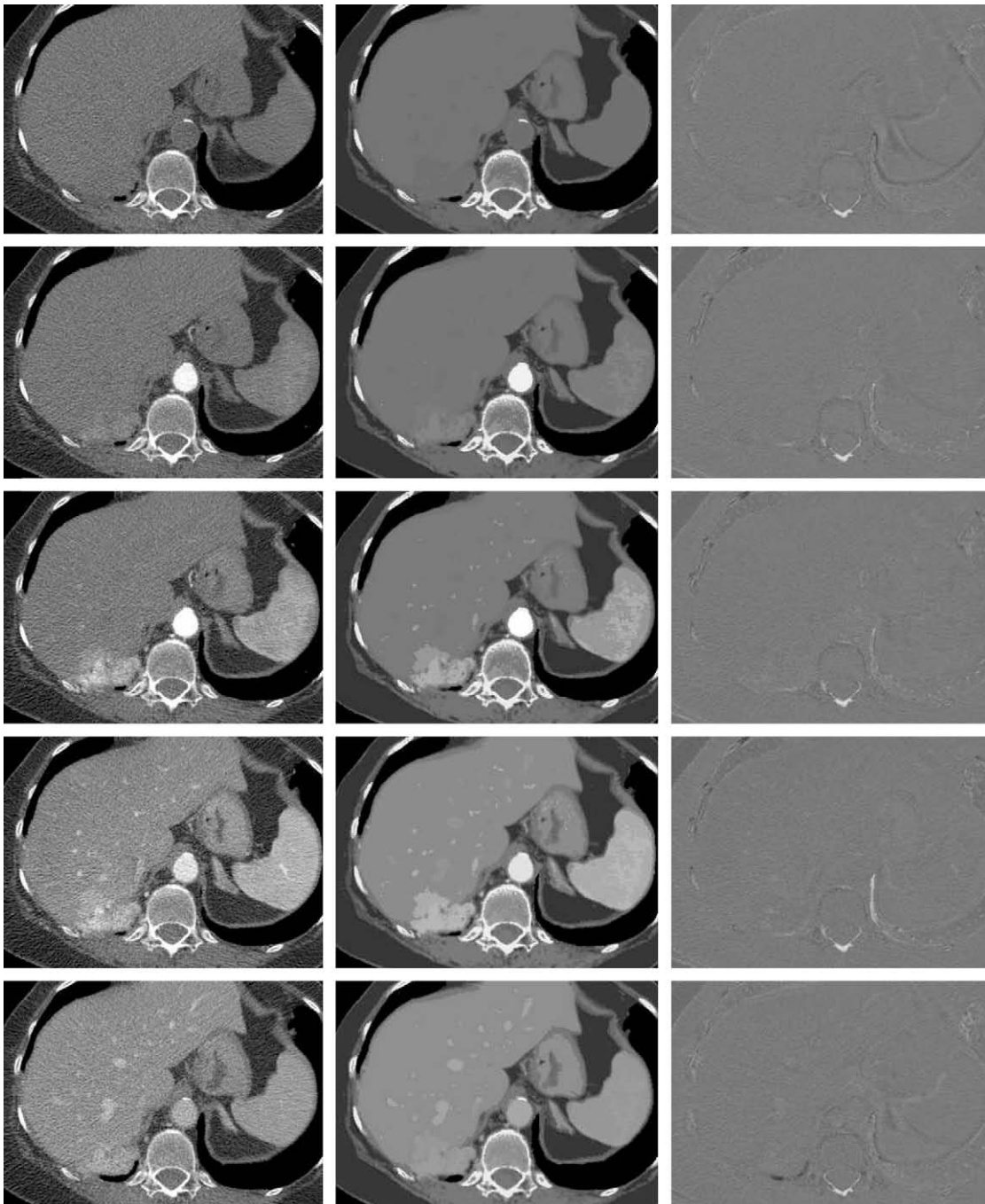


Fig. 5. An abdominal DET-CT scan sequence of the first patient. Some images of the original sequence (first column), the estimated template (second column), and differences between original images and registered template frames (third column).

tained on two typical sequences, one of the upper abdomen (first patient) and another of the thorax (second patient). Some selected images of these sequences are presented on first columns of Figs. 5 and 6.

For each sequence, images were acquired at the same axial level with an in-plane resolution of 512×512 pixels. For the abdominal sequence (53 images), images were acquired at three uniformly sampled intervals of time, corresponding to periods of apnea. For the thoracic sequence, images were acquired every second after the contrast agent injection. We only used the first 30 images, in which the main intensity variations are observed. In addition, an

iodinated contrast media was injected to enhance the vascular properties of tissues. The anatomy underlying the sequences is briefly described in Fig. 7.

The contrast agent injection enables us to enhance and observe some classes which are not visible before injection, e.g. veins and tumors. However, images suffer from a poor signal-to-noise ratio, due to the limited irradiation dose used for the sequential acquisition (acquisition parameters were fixed at 80 Kv and 50 mAs). Besides, observed tissues were deformed during the sequence, due to the patient breathing, heart pulsations, gastric contractions and some possible voluntary movements.

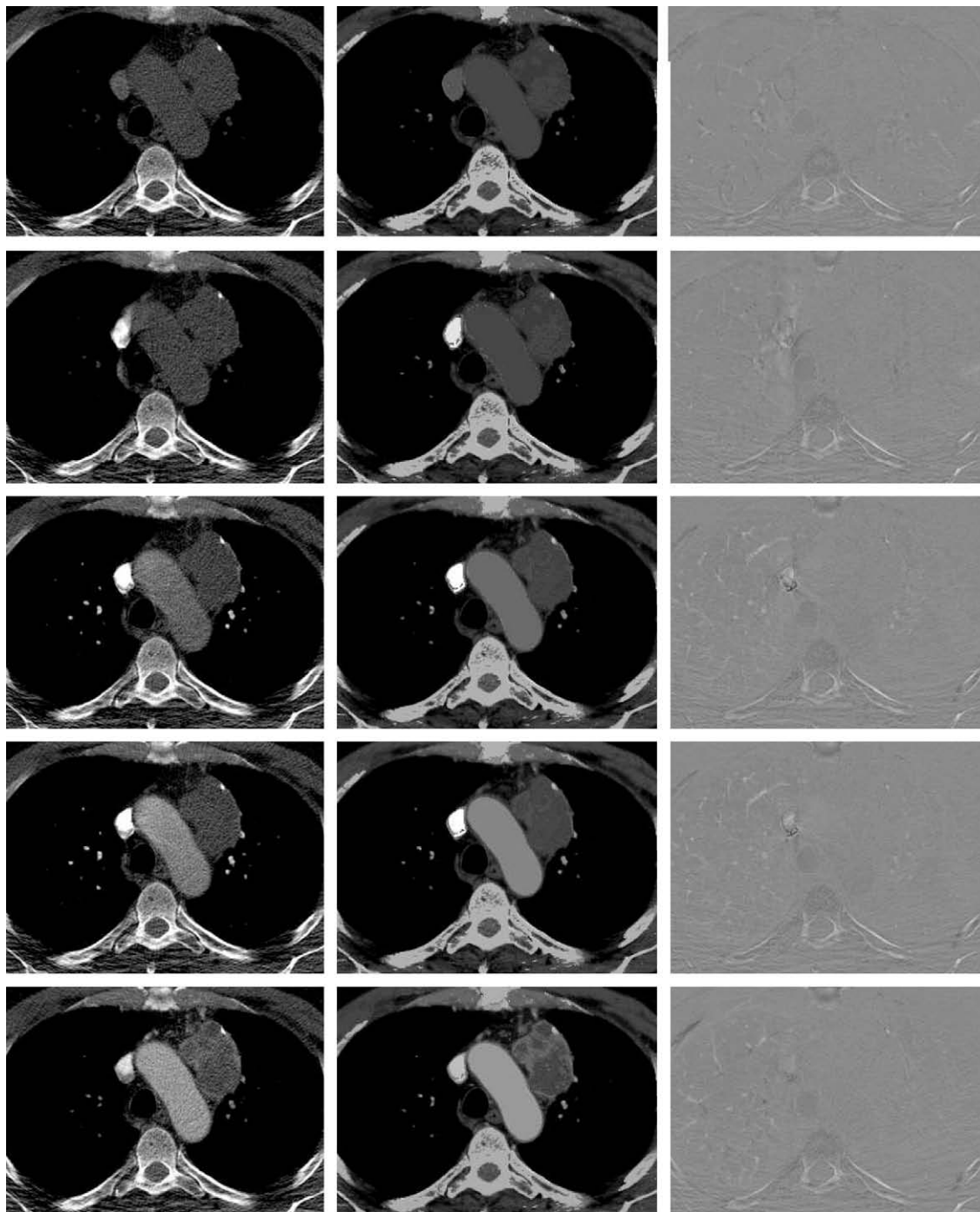


Fig. 6. A thoracic DET-CT scan sequence of the second patient. Some images of the original sequence (first column), the estimated template (second column), and differences between original images and registered template frames (third column).

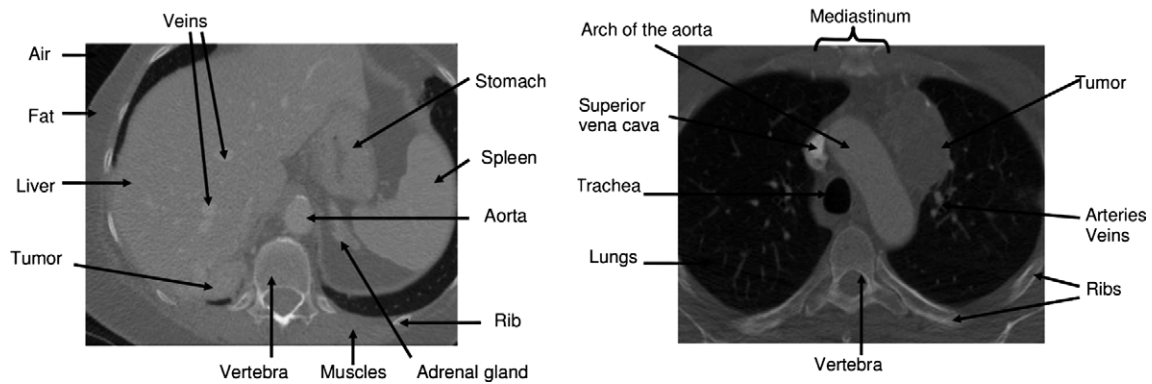


Fig. 7. A brief anatomical description of CT-scans of the abdomen and the thorax.

In Figs. 8 and 9, we show classifications and associated enhancement curves obtained before and after the application of our technique. Enhancement curves result from averaging gray-level values of pixels of each class at each time. They are shown in Hounsfield Units (UH).

In the first sequence, enhancement curves drawn before registration have peaks at 35 and 75 s, corresponding to the patient breathing after periods of apnea. These peaks are well attenuated by the registration. In the second sequence, we notice that enhancement curves which correspond to different tissue classes are well separated after registration. For instance, after registration, we can distinguish four classes of pixels whose contrast curves are among the highest. Those classes correspond to the arch of aorta, the superior vena cava and compact bones. This anatomical segmentation is obtained as a result of the creation of interface classes whose initial intensities vary between -400 and 0 , notably, associated to lungs borders. As shown on the first sequence, the technique obtained several classes of pixels on the tumor and on the fail (see Fig. 8). Such a result is anatomically sound because:

(1) the tumor is composed of vascular and cell parts having different dynamic behaviors and (2) the fail is a tissular component composed of red and white pulps with different vascularisations. The algorithm also obtained two pixel classes for the vena cava (see Fig. 9). This can be explained by the fact that, when they arrive in the vena cava, the contrast agent and the blood are not mixed yet, and have different dynamic behaviors. Those classification results suggest that pixel classifications are consistent with the anatomy and that the technique is accurate enough to distinguish subtle dynamic properties of tissues.

Up to now, we have observed three kinds of improvements due to the registration block of our technique:

- Some inconsistent classes containing unregistered pixels having behaviors similar to real dynamic enhancements were removed after registration (Fig. 10).
- Some inconsistent classes present before registration were corrected after registration. For instance, after registration of the abdominal sequence, there is a unique class corre-

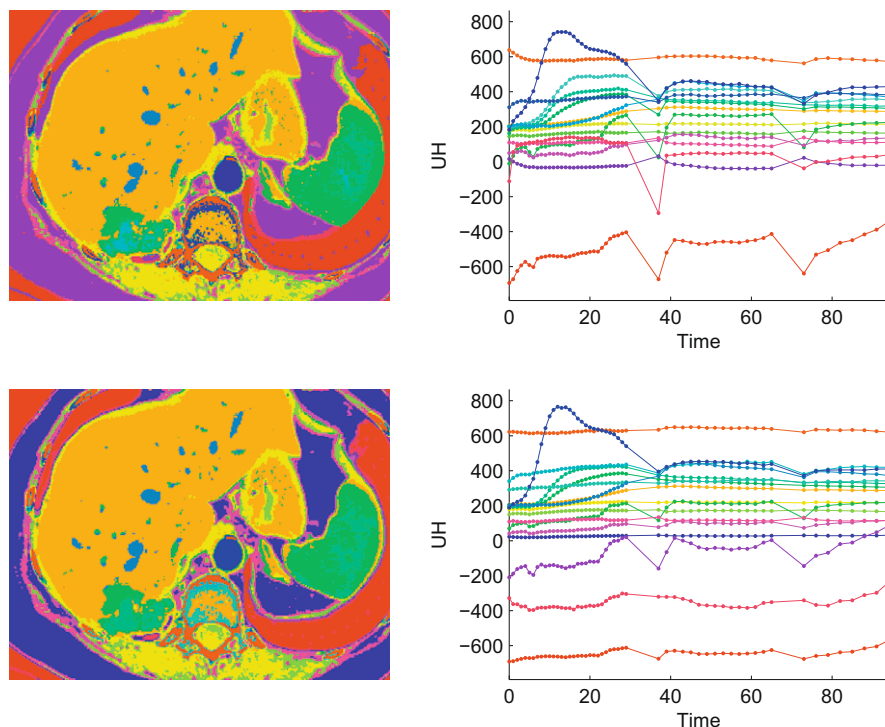


Fig. 8. An abdominal sequence: classifications obtained before (first line) and after registration (second line), and associated dynamic enhancement curves (UH versus time).

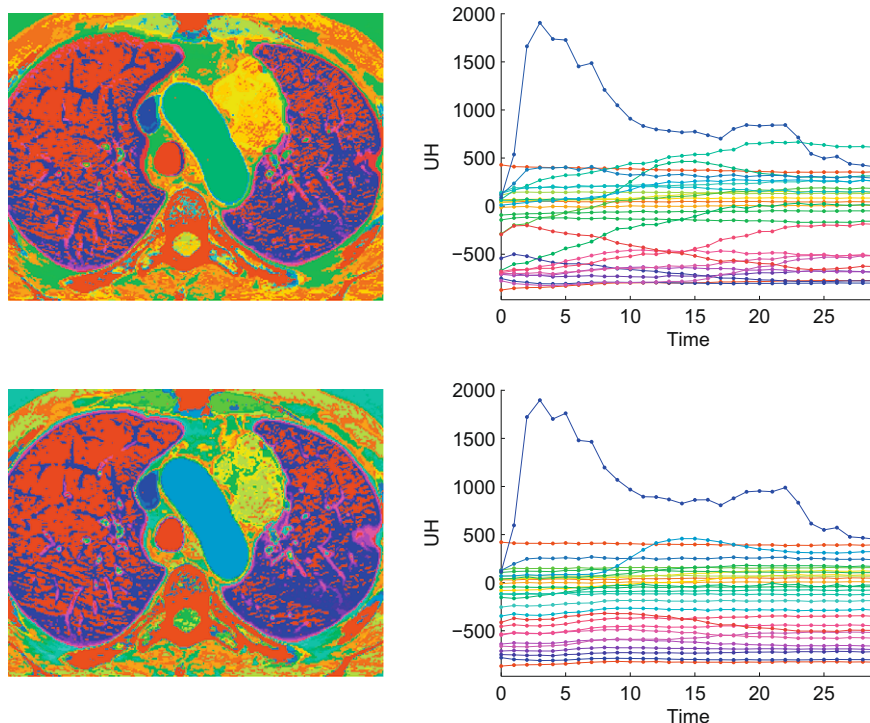


Fig. 9. A thoracic sequence: classifications obtained before (first line) and after registration (second line), and associated dynamic enhancement curves (UH versus time).

sponding to fat whereas before registration, the fat class also includes some pixels of the air and the liver located in the upper-left side.

- Some new classes appeared after registration. This is particularly the case for the interface classes (see Figs. 8 and 9).

In Figs. 5 and 6, we show some images of original sequences, together with the estimated temporal templates, and the difference images between original images and registered template frames.

On these images, we notice that temporal templates capture the main dynamic enhancement features of the sequences. In the first sequence, the aorta, which takes contrast first, is followed by the lesion and veins. In the second sequence, vena cava takes contrast first and the arch of aorta is second.

Besides, due to the estimation of contrast curves on classes, the noise present in the initial images is filtered and appears attenuated in templates.

As it can be noticed in Figs. 5 and 6, the fitting of the original images and the registered estimated template is quite accurate. However, there are still some differences between those images and the template. For instance, on the first sequence, we notice some differences due to topology changes on the right side of ver-

tebra (two separated parts are merged). We also observe some differences in the air located in superior right side of images in both sequences. This is due to the fact that corresponding classes are not homogeneous and have relatively high standard deviation. This is also the case of the superior vena cava on the second sequence.

For a quantitative evaluation of the registration, we applied the following procedure. We chose m images of the original sequence ($m = 6$) associated with times t_1, \dots, t_m . On each selected image J^i , we located manually a set of predefined anatomical regions: we denote by S_j^i the set of pixels of the segmented regions. Each segmentation S_j^i is then transported on the other images J^i ($i \neq j$) using the deformations obtained by registration. For any i and j in $1, \dots, m$ such that $i \neq j$, we obtained the transported segmentations:

$$S_{j,i} = (\phi^i)^{-1}(\phi^j(S_j^i)) \cap \Omega_d.$$

Next, we compared the transported segmentations to the manual segmentations using a criterion of misclassified pixels: $\text{Card}(S_j^i \Delta S_{j,i})$ where Δ denotes the symmetric difference of two sets ($A \Delta B = (A \cap B^c) \cup (A^c \cap B)$). The overall mean error is computed as

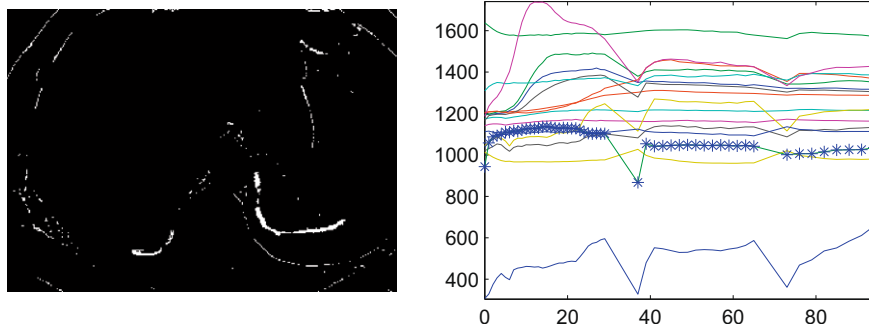


Fig. 10. Example of a pixel class removed after registration.

$$Err = \frac{1}{m(m-1)} \sum_{i=1}^m \sum_{j=1, j \neq i}^m \text{Card}(S_i^* \Delta S_{j,i}).$$

To compare segmentations of regions having different sizes, we also compute the mean of the *Jaccard coefficient* Tan et al. (2006). This criterion, which quantifies the overlap between two sets X et Y by a normalized value J_C , has a value between 0 and 1:

$$J_C = \frac{\text{Card } X \cap Y}{\text{Card } X \cup Y}.$$

So, the overall segmentation quality can also be evaluated by a normalized value J_{C_m} which is independent of region size variations

$$J_{C_m} = \frac{1}{m(m-1)} \sum_{i=1}^m \sum_{j=1, j \neq i}^m \frac{\text{Card}(S_i^* \cap S_{j,i})}{\text{Card}(S_i^* \cup S_{j,i})}.$$

The registration evaluation is done by comparing segmentation results obtained before and after registration. Results are reported

Table 1
Quantitative registration evaluation on the sequence of the first patient.

Region	Err		J_{C_m}	
	Before reg.	After reg.	Before reg.	After reg.
Aorta	50.7	54.3	0.917	0.911
Stomach	458.4	288.1	0.865	0.912
Liver	973.6	651.6	0.964	0.976
Lesion	313.4	258.5	0.794	0.825
Spleen	739	310.8	0.865	0.940

Table 2
Quantitative registration evaluation on the sequence of the second patient.

Region	Err		J_{C_m}	
	Before reg.	After reg.	Before reg.	After reg.
Aorta	209.3	200.7	0.950	0.952
Trachea	77.5	27.5	0.859	0.946
Lungs	1097.7	426.7	0.948	0.979
Tumor	342.9	317.0	0.903	0.910

Table 3
Quantitative registration evaluation on sequences of the third patient. The values are obtained by averaging the results of the registration of four sequences located at four different axial levels.

Region	Err		J_{C_m}	
	Before reg.	After reg.	Before reg.	After reg.
Aorta	56.3	55.1	0.904	0.906
Stomach	473.3	395.1	0.858	0.880
Lesion	209.6	194.5	0.859	0.862
Spleen	180.3	183.1	0.949	0.949

Table 4
Quantitative registration evaluation on sequences of the fourth patient (abdominal sequences). The values are obtained by averaging the results of the registration of five sequences located at five different axial levels.

Region	Err		J_{C_m}	
	Before reg.	After reg.	Before reg.	After reg.
Ascending aorta	494.9	332.2	0.822	0.876
Trunk	1133.3	831.0	0.821	0.864
Lungs	2019.8	1489.1	0.966	0.975
Superior vena cava	280.7	161.6	0.5367	0.691

in Tables 1 and 2 for the two patient sequences used previously and in Tables 3 and 4 for sequences of the two other patients.

From Tables 1–4, we can say that our new technique improves the segmentation results by reducing the number of badly classified pixels, especially for regions which are significantly moving and characterized by a low Jaccard coefficient before registration. This is specially the case for the spleen, the stomach, and the lesion of the first patient, and lungs and trachea of the second patient. On relatively stable regions such as the aorta, the new technique gives similar segmentation results to those obtained before registration.

4. Discussion and conclusion

The estimation of contrast enhancement curves from DCE sequences is a difficult problem due in particular to possible movements occurring in sequences. The contrast agent and patient movements generate two different types of image transformations within sequences: whereas the first one causes intensity transformations modifying gray-level values of successive images, the second ones cause deformations changing only the geometry of tissues. Hence, the main difficulty of the problem is to distinguish both types of transformations. From a mathematical point of view, this difficulty is related to the fact that the problem of estimating enhancements and registering the sequence at the same time is ill-posed. Without any constraint on possible enhancements nor on deformations, the problem has a wide choice of possible solutions. As a consequence, a geometrical deformation may not be corrected by registration but instead, it can be seen as a contrast change and compensated for by enhancement estimation.

In the construction of our new technique, we use several constraints which aim at avoiding such an error and restricting relevantly the field of possible solutions of the problem. First, enhancement curves are estimated on classes of pixels instead of single pixels. In a class, some unregistered pixels are generally mixed with numerous correctly registered pixels. Hence, their influence on the curve estimation is restricted due to a mean effect on the class. As a consequence, a class-based estimation is less sensitive to mis-registered pixels than usual pixel-based estimations. Due to the estimation on classes, our technique should be faster than other pixel-based techniques where curves are estimated for each pixel of images (Hayton et al., 1997).

Besides, we carefully introduced some constraints in steps of the classification scheme itself. For splitting classes at each level of the tree classification step, we designed a modified version of the K-means algorithm. In this algorithm, centers of the class are parametrized by some heuristic curves so as to ensure that several features of centers are consistent with those we expect from dynamic enhancements. Moreover, the classification scheme ends with a pruning step which removes some possible inconsistent classes using a simple criterion on the shape of class centers.

As a preliminary step of our work, the technique presented here was implemented in 2D. Hence, the obtained registrations do not correct the vertical movements of the patients. In the future, we plan to fix this drawback. Notice however that a 3D implementation of our technique only requires modifying the registration part to take into account vertical deformations, and is quite straightforward.

The technique we propose relies upon a generic architecture which is based on two blocks (classification and registrations). Although they interact through input and output, these blocks are independently defined and can be modified separately. In particular, it is possible to improve the classification using more efficient techniques (e.g. forests Biau et al. (2008)) and adding a homogenization post-processing stage without changing the overall architecture of the technique.

Our technique relies upon the assumption that class intensities are homogeneous. This is true for the CT-scan we dealt with but

not necessarily for modalities such as MRI or PET where the partial volume effect is critical. For the application to such modalities, our technique should be modified to take into account the statistical heterogeneity of each class using specific estimation and classification methods (e.g. texture modeling and analysis, mixture models, robust statistics, . . .). In particular, for dynamic PET sequences, we plan to incorporate the classification technique of Maroy et al. (2008) in the block (T) of our algorithm.

References

- Biau, G., Devroye, L., Lugosi, G., 2008. Consistency of random forests and other averaging classifiers. *Journal of Machine Learning Research* 9, 2015–2033.
- Buonaccorsi, G., Roberts, C., Cheung, S., Watson, Y., O'Connor, J., Davies, K., Jackson, A., Jayson, G., Parker, G., 2006. Comparison of the performance of tracer kinetic model-driven registration for dynamic contrast enhanced MRI using different models of contrast enhancement. *Academic Radiology* 13 (9), 1112–1123.
- Cuénod, C., Fournier, L., Balvay, D., et al., 2006. Tumor angiogenesis: pathophysiology and implications for contrast-enhanced MRI and CT assessment. *Abdominal Imaging* 31 (2), 188–193.
- Duda, R., Hart, P., Stork, D., 2000. *Pattern Classification*, second ed. Wiley-Interscience.
- Hachama, M., 2008. Modèles de recalage classifiant pour l'imagerie médicale. Ph.D. Thesis, University Paris Descartes.
- Hachama, M., Desolneux, A., Richard, F., 2006. Combining registration and abnormality detection in mammography. In: *Proceedings of the Workshop on Biomedical Image Registration*. pp. 178–185.
- Hayton, P., Brady, M., Tarassenko, L., Moore, N., 1997. Analysis of dynamic MR breast images using a model of contrast enhancement. *Medical Image Analysis* 1, 207–224.
- Hecht, F., 2008. FREEFEM++. Université Pierre et Marie Curie, Paris, Laboratoire Jacques-Louis Lions, third ed. <<http://www.freefem.org/ff++/index.htm>>.
- Henkjan, H., Engelbrecht, M., Barentsz, J., 2001. Accurate estimation of pharmacokinetic contrast-enhanced dynamic MRI parameters of the prostate. *Journal of Magnetic Resonance Imaging* 13 (4), 607–614.
- Judd, R., Lugo-Olivieri, C., et al., 1995. Physiological basis of myocardial contrast enhancement in fast magnetic resonance images of 2-day-old reperfused canine infarcts. *Circulation* 92 (7), 1902–1910.
- Kaiser, W., 1990. Dynamic magnetic resonance breast imaging using a double breast coil: an important step towards routine examination of the breast. *Frontiers in European Radiology* 7, 39–68.
- Kuhl, C., 2007. The current status of breast MR imaging. Part I. Choice of technique, image interpretation, diagnostic accuracy, and transfer to clinical practice. *Radiology* 244 (2), 356–378.
- Lorenzo, L., MacLeod, R., Whitaker, R., Adluru, G., DiBella, E., 2006. Level sets and shape model for segmentation of cardiac perfusion MRI. In: Reinhardt, J.M., Plum, J. (Eds.), *Proceedings of the SPIE Medical Imaging'2006*, vol. 6144. San Diego, CA, pp. 1320–1331.
- Maroy, R., Boisgard, R., Comtat, C., Frouin, V., Cathier, P., Duchesnay, E., Dolle, F., Nielsen, P., Trebossen, R., Tavitian, B., 2008. Segmentation of rodent whole-body dynamic PET images: an unsupervised method based on voxel dynamics. *IEEE Transactions on Medical Imaging* 27 (3), 342–354.
- Miles, K., 2003. Perfusion CT for the assessment of tumor vascularity: which protocol? *The British Journal of Radiology* 1 (76), 36–42.
- Moate, P., Dougherty, L., Schnall, M., et al., 2004. A modified logistic model to describe gadolinium kinetics in breast tumors. *Magnetic Resonance Imaging* 22 (467–473).
- Mussurakis, S., Buckley, D., Bowsley, S., et al., 1995. Dynamic contrast-enhanced magnetic resonance imaging of the breast combined with pharmacokinetic analysis of gadolinium-DTPA uptake in the diagnosis of local recurrence of early stage breast carcinoma. *Investigative Radiology* 30 (11), 650–662.
- O'Connor, J., Jackson, A., Parker, G., Jayson, G., 2007. DCE-MRI biomarkers in the clinical evaluation of antiangiogenic and vascular disrupting agents. *British Journal of Cancer* 2 (96), 189–195.
- Padhani, A., 2002. Dynamic contrast-enhanced MRI in clinical oncology: current status and future directions. *Magnetic Resonance Imaging* 16 (4), 407–422.
- Roche, A., Malandain, A., Ayache, N., 2000. Unifying maximum likelihood approaches in medical image registration. *International Journal of Computer Vision of Imaging Systems and Technology* 11, 71–80.
- Rougon, N., Discher, A., Preteux, F., August 2005. Region-driven statistical non-rigid registration: application to model-based segmentation and tracking of the heart in perfusion MRI. In: *Proceedings SPIE Conference on Mathematical Methods in Pattern and Image Analysis*, vol. 5916. San Diego, pp. 148–159.
- Schmid, V., Whitther, B., Yang, G., et al., 2005. Statistical analysis of pharmacokinetic models in dynamic contrast-enhanced magnetic resonance imaging. In: *Medical Image Computing and Computer Assisted Intervention (MICCAI05)*, vol. 8. pp. 886–893.
- Stack, J., Redmond, O., Codd, M., et al., 1990. Breast disease: tissue characterisation with GD-DTPA enhancement profiles. *Radiology* 174, 491–494.
- Tan, P.-N., Steinbach, M., Kumar, V., 2006. *Introduction to Data Mining*. Addison-Wesley.
- Tofts, P., 1997. Modeling tracer kinetics in dynamic Gd-DTPA MR imaging. *Journal of Magnetic Resonance Imaging* 7 (1), 91–101.
- Wintermark, M., 2005. Brain perfusion-CT in acute stroke patients. *European Radiology Supplements* 15 (4), d28–d31.
- Xiaohua, C., Brady, M., Lo, J., Moore, N., 2005. Simultaneous segmentation and registration of contrast-enhanced breast MRI. In: *Information Processing in Medical Imaging*. pp. 126–137.
- Zahra, M., Hollingsworth, K., Sala, E., et al., 2007. Dynamic contrast-enhanced MRI as a predictor of tumour response to radiotherapy. *The Lancet Oncology* 8 (1), 63–74.